Constraining the chemical and mineralogical composition of Earth's lower mantle through high-pressure crystallography and mineral elasticity

Giacomo Criniti
Bayerisches Geoinstitut, University of Bayreuth, Universitätsstraße 30, 95447, Bayreuth, Germany
DOI: 10.19276/plinius.2025.01.009

THE EARTH'S DEEP INTERIOR

The Earth's lower mantle, spanning from approximately 660 to 2890 km depth, comprises more than half of the total volume of the Earth. Due to its inaccessibility and the lack of pristine natural samples reaching the surface from such great depths, some of its key properties, such as bulk chemical composition and temperature, need to be inferred from the interpretation of geophysical observations. It is the role of high-pressure experiments to provide the tools necessary to retrieve this information by investigating the phase equilibria, mineral transformations, and physicochemical properties of candidate lower mantle phases.

Seismic models and laboratory experiments

On first approximation, the geophysical properties of the Earth's deep interior, such as its density and seismic velocities, have been approximated as spherically symmetrical. One-dimensional (1D) seismic models, such as the preliminary reference Earth model (Dziewonski & Anderson, 1981), have therefore been used by experimentalists to infer the average chemical composition of the deep Earth, including the lower mantle. Phase equilibrium experiments on bulk rock compositions ranging from harzburgite to basalt at lower mantle pressure and temperatures have revealed bridgmanite, $(Mg,Fe,Al)(Si,Al)O_3$ with a distorted perovskite-type structure, to be the most abundant mineral phase down to at least 2700 km depth. Its abundance relative to (Mg,Fe)O ferropericlase, the second most abundant mineral, remains, however, controversial. For the past several decades, extensive efforts have been put into measuring the density and wave propagation velocities of candidate lower mantle phases. The most utilized technique has been Brillouin scattering, which can be coupled to diamond anvil cells (DACs) to measure velocities up to conditions of the deep lower mantle. Technological and experimental challenges, however, have often limited the effective pressure and temperature range in which such properties can be measured. For instance, the Brillouin signal from the diamond anvils tends to mask the compressional velocities of minerals at lower mantle pressures, limiting observations to only the shear velocities. It follows that the accuracy and precision of mineral physical models used to interpret 1D seismic models has not allowed us to apply robust constraints on the average lower mantle composition and temperature yet.

Water in the deep Earth

Hydrogen, often expressed as its oxide component H_2O and simply referred to as "water", is a minor, yet crucial component of mantle rocks. It can significantly lower their solidus temperature, enhance their thermal and electrical conductivity, as well as reduce their viscosity.

Dense hydrous magnesium silicates (DHMS) are synthetic phases that appear in high-pressure-temperature experiments on hydrous mafic and ultramafic compositions from upper to lower mantle conditions. They are believed to be the primary water carriers within subducted oceanic plates down to the mantle transition zone but are believed to dehydrate in the shallow lower mantle due to their limited thermal stability (Frost, 2006). Owing to a coupled substitution of Mg^{2+} and Si^{4+} by Al^{3+}, super-aluminous equivalents of phase D ($MgSi_2O_6H_2$) and phase H ($MgSiO_4H_2$) were found to survive up to temperatures approaching or even exceeding those of the ambient mantle geotherm (Pamato et al., 2015). Constraining their physical properties can therefore improve our understanding of the seismic signature of water within rocks deep inside the Earth.

Out of the nominally anhydrous minerals that have been studied so far, stishovite, a high-pressure polymorph of SiO_2 and major component of meta-basaltic rocks at lower-mantle conditions, was shown to have the highest water storage capacity, exceeding 1 wt.% H_2O (*e.g.*, Ishii et al., 2022). The coupled substitution of Si^{4+} by Al^{3+} and H^+ has recently drawn significant attention as

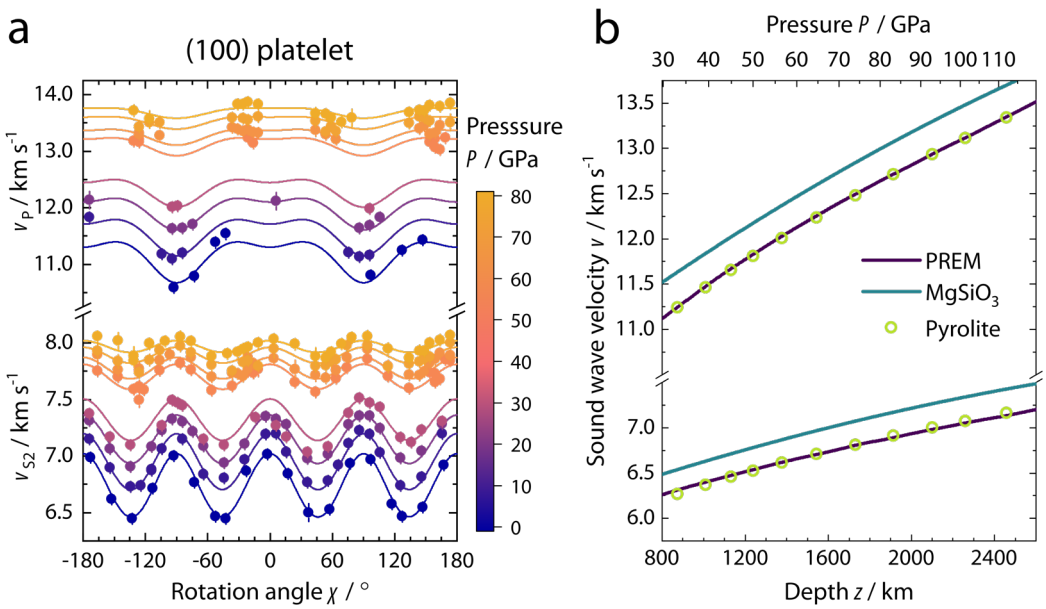

Figure 1 a) *Measured shear (v_{S2}) and compressional (v_P) velocities of a platelet of $MgSiO_3$ bridgmanite (symbols) and calculated dispersion curves calculated from the global inversion (lines) as a function of pressure (color scale) in the (100) crystal platelet.* ***b)*** *Seismic velocities in the lower mantle according to PREM and calculated velocities of $MgSiO_3$ bridgmanite (teal line) from this thesis and of a pyrolite phase assemblage (green symbols) as a function of depth along an adiabatic temperature profile.*

it was found to also affect the stability and elastic properties of stishovite. In fact, it reduces the pressure at which stishovite undergoes a structural phase transition to so-called post-stishovite, or $CaCl_2$-type SiO_2, where both phases experience extensive shear elastic softening. These elastic anomalies in silica phases with different Al and H contents could explain a series of seismic scatterers detected in the shallow- to mid-lower mantle in the proximity of subducted slabs (Kaneshima, 2019).

Aim of this thesis

The scope of this thesis is twofold: *i)* to improve our understanding of the composition of the ambient mantle by accurately determining the thermoelastic properties of bridgmanite, its most abundant mineral; and *ii)* to seek potential "water signatures" in the seismic properties of water-bearing silicates in lower-mantle basaltic phase assemblages. To this end, diamond anvil cell experiments were conducted to determine the high-pressure single-crystal elasticity of $MgSiO_3$ bridgmanite, the thermal equation of state of Al-bearing bridgmanite, the pressure-induced phase transformation of H,Al-bearing SiO_2 stishovite, and the compressibility of Mg-free Al-phase D.

ACOUSTIC VELOCITIES OF $MgSiO_3$ BRIDGMANITE IN THE MID-LOWER MANTLE

High-pressure measurements of the sound velocities of mantle minerals by Brillouin scattering in diamond anvil cell (DAC) are often impeded by the overlap of the compressional velocities (v_P) of the sample with the much more intense shear velocity (v_S) of diamond anvils (Kurnosov et al., 2017; Murakami et al., 2012). Because sound velocities vary depending on propagation and polarization directions in single-crystalline materials, it is possible to tune the reciprocal orientation of diamond anvils and single-crystal bridgmanite samples to minimize the overlap between the two peaks in Brillouin spectra. To this end, I developed a protocol to prepare bridgmanite samples for Brillouin scattering measurements in the DAC that allowed me to determine for the first time the full elastic tensor of $MgSiO_3$ bridgmanite up to ~80 GPa (Fig. 1a), corresponding to pressures of the mid-lower mantle. While at pressures below 30 GPa the bridgmanite v_P was observed in a few directions, at the diamond v_S maxima, above 50 GPa a crossover was observed at the diamond v_S minima, thus providing us with the first experimental constraints on the v_P of any bridgmanite composition at such high pressures.

Finite-strain equations of state describing how the elastic coefficients of bridgmanite (c_{ij}) vary with volume were employed in a simultaneous inversion of all diffraction and Brillouin data. This allowed gaps in the high-pressure data to be filled by using constraints from the low-pressure data, and vice versa. It also allowed the c_{ij}, as well as the bulk (K) and shear (G) moduli, to be calculated throughout the entire pressure range investigated by just refining a set of fit parameters for each c_{ij} equation of state (c_{ij0}, c'_{ij0}) instead of a set of 9 c_{ij} at each pressure.

The high-pressure sound velocity data obtained here were subsequently combined with previously published velocity data sets collected at high pressure and temperature by ultrasonic interferometry in the multi-anvil press to reassess the thermoelastic parameters of the $MgSiO_3$ bridgmanite end member (Fig. 1b). Together with experimental and theoretical results from previous studies on other lower mantle minerals (*e.g.*, Stixrude & Lithgow-Bertelloni, 2005) and thermodynamic data on the Fe^{2+}-Mg partitioning between bridgmanite and ferropericlase (Nakajima et al., 2012), an internally consistent mineral physical model was built. This model was used

to calculate the sound wave velocities of a simplified pyrolite composition along an adiabatic temperature profile at lower mantle depths and compare them with 1D seismic models of the lower mantle. Although simplified, the model is in excellent agreement with seismic data (Fig. 1b), suggesting that the chemical compositions of the upper and lower mantle may not be as dissimilar as previously proposed (Murakami et al. 2012).

EFFECT OF AL SUBSTITUTIONS ON THE THERMOELASTICITY OF BRIDGMANITE

The occurrence of vacancies in the oxygen sublattice of bridgmanite has been known for decades (Navrotsky et al., 2003). To accurately quantify the effect of the oxygen-vacancy (OV) $MgAlO_{2.5}$ substitution mechanism against that of the charged-couple (CC) $AlAlO_3$ mechanism, measurements of well-characterized, high-quality single crystals are critical. Here, we synthesized four aluminous bridgmanite samples at shallow lower mantle conditions in a multi-anvil press and characterized them *in-house* by electron microprobe and single-crystal X-ray diffraction at ambient conditions. Al contents ranged from 0.10 to 0.18 per formula unit, with molar fractions of the OV component from 2% to 5%.

Three of the four samples were subsequently loaded in resistive-heated DAC and single-crystal X-ray diffraction measurements were carried out at the synchrotron beamline P02.2 of Petra-III (Hamburg, Germany) up to 80 GPa at room temperature and up to 30 GPa and 1000 K at combined high pressure and temperature. A 3rd-order Birch-Murnaghan equation of state with the thermal pressure model formulated by Stixrude & Lithgow-Bertelloni (2005) was employed to fit the experimental pressure-volume-temperature data sets (Fig. 2a).

From the analysis of the molar volumes and bulk moduli of Al-bearing bridgmanite samples reported in this and previous studies, no apparent divergence between trends described along the CC and OV joins were found (Fig. 2b), despite previous studies reporting significantly larger molar volume and smaller bulk modulus for the $MgAlO_{2.5}$ component. Therefore, the presence of 5 mol.% OV component in bridgmanite, compatible with the concentrations expected in a pyrolitic lower mantle (Huang et al., 2021), likely has a negligible effect on the seismic properties of bridgmanite. By comparing the compression behavior of the whole structure and that of its individual crystallographic sites, it further appears that the main factor influencing the compressibility of aluminous bridgmanite is the Al content in the octahedral site.

The experimental results obtained here were then used to extrapolate previously determined phase equilibria in the MgO-$AlO_{1.5}$-SiO_2 system to explore how pressure and temperature affect the concentration of the OV component in bridgmanite down to mid-lower mantle

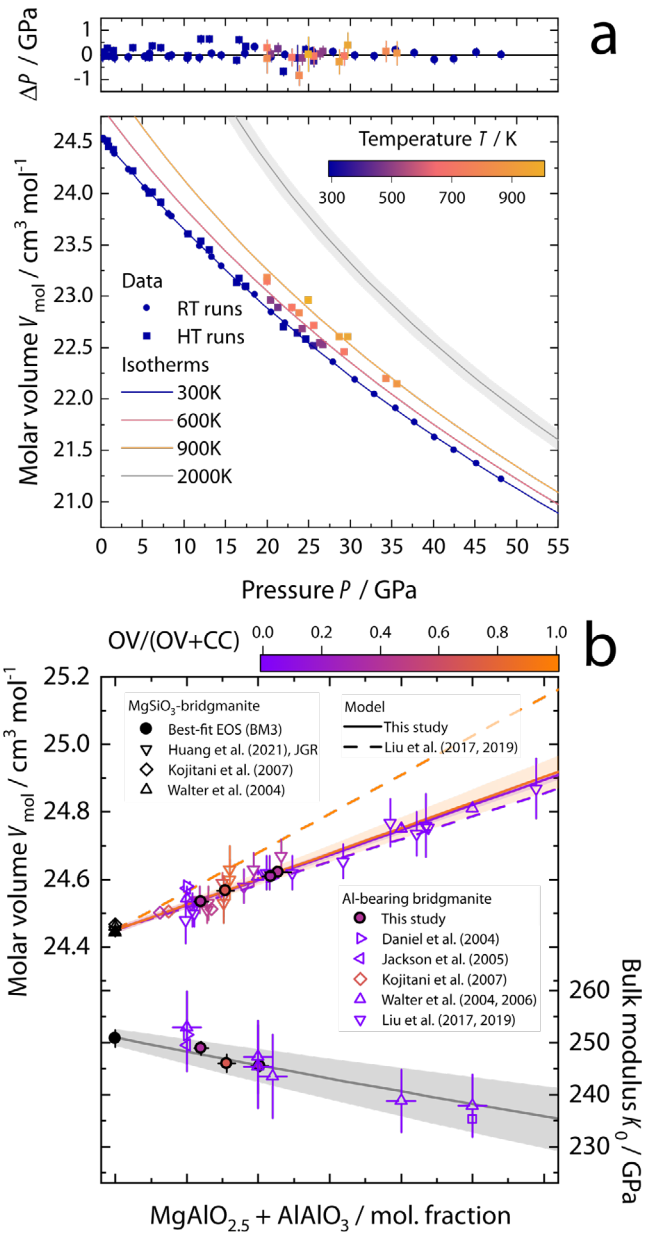

Figure 2 a) *Measured volumes for bridgmanite sample CC2-OV5 as a function of pressure and temperature (color scale), and calculated isotherm at selected temperatures. The 2000 K isotherm also displays the propagated uncertainty from the fit parameters. At the top, the difference between the measured and calculated pressures (ΔP).* ***b)*** *Measured and modelled molar volume (top) and bulk modulus (bottom) of bridgmanite along the $MgSiO_3$-$AlAlO_3$ and $MgSiO_3$-$MgAlO_{2.5}$ joins. Ratios of CC and OV components are expressed by the color scale. At the bottom, the two Al-end members were assumed to have the same bulk modulus, and the fitted curve is represented in gray instead of the purple-orange color coding. Shaded areas represent propagated uncertainties from a three- (top) or two-end-member model (bottom).*

conditions. From a reanalysis of literature data at 27 GPa and 2000 K, the standard-state Gibbs free energy (ΔG^0) and interaction parameter of Si and Al in the B-site of bridgmanite (W_{SiAl}^{B}) were refined. Extrapolation to higher pressures using the newly determined thermoelastic parameters of aluminous bridgmanite produced a much better agreement with the few available literature data than previous computational estimates (Brodholt, 2000). When included in more complete models, considering the effects of Fe and oxygen fugacity, the thermoelas-

tic and thermodynamic parameters reported here will enable more reliable estimates for the composition of bridgmanite and coexisting ferropericlase at shallow- to mid-lower mantle conditions to be obtained.

ANOMALOUS BEHAVIOR OF H,AL-BEARING SILICA PHASES UNDER PRESSURE

Although H and Al are known to expand the stability field of post-stishovite at the expense of that of stishovite, their individual and combined effects have not yet been disentangled. Recently, we found Al-bearing silica synthesized at 2200 K and 28 GPa not only to incorporate more than 1 wt.% H_2O but also to retain the $CaCl_2$-type structural modification of post-stishovite upon decompression to ambient conditions (Ishii et al., 2022), suggesting H plays a crucial role in stabilizing post-stishovite. To better understand the relation between Al and H incorporation, phase stability and physical properties, single-crystal synchrotron X-ray diffraction, structural refinements, and Raman spectroscopy measurements were conducted in the DAC up to 50 GPa on two samples of tetragonal $Al_{0.05}Si_{0.95}O_{1.98}H_{0.02}$ (Al5) and orthorhombic $Al_{0.11}Si_{0.89}O_{1.97}H_{0.07}$ (Al11).

Upon compression to about 16 GPa, the symmetry of Al5 changed from tetragonal to orthorhombic, whereas the Al11 sample preserved its orthorhombic symmetry throughout the entire pressure range investigated. The structure of the two samples was refined at every pressure point, and the amplitude of the symmetry-breaking structural mode Γ_2^+, related to the octahedral tilt angle, was calculated. In a pseudo-proper ferroelastic transition, as in SiO_2 stishovite, the tilt angle increases linearly with pressure (Zhang et al., 2023). Our results, however, highlight a concave rather than linear evolution (Fig. 3a), suggesting that another mechanism could also be involved in the transition. Additionally, the evolution of the Raman active soft mode associated with the post-stishovite transition displayed a different behavior from previously studied SiO_2 and aluminous stishovite samples (*e.g.*, Zhang et al., 2021). When the squared wavenumber (ω^2) is plotted against pressure, instead of changing abruptly at the transition pressure, ω^2 of the Al5 sample was found to decrease up to 20 GPa (*i.e.*, past the crystallographic transition pressure), then remain constant for approximately 10 GPa, and finally increase only above 30 GPa (Fig. 3b). An interval with weak-to-no pressure dependence of the soft mode was also found in the Al11 sample, whose symmetry is orthorhombic already from room pressure (Fig. 3b). Given the higher hydrogen content of our samples with respect to samples described in previous studies, and the fact that a symmetrization of the hydrogen (H-) bonds follows the Γ_2^+ symmetry-breaking structural mode, we concluded that the coupled substitution $Si^{4+} = Al^{3+} + H^+$ is much more efficient in decreasing the transition pressure of stishovite to post-stishovite than the oxygen vacancy substitution $Si^{4+} = Al^{3+} + 1/2OV^{2-}$.

It is still unclear at what pressure elastic anomalies are expected to occur in H,Al-bearing silica, whether at the onset of the crystallographic phase transition from or throughout the Raman soft mode plateau. Depending on which scenario is considered, and assuming the phase transition has a Clapeyron slope of 89 K/GPa (Nomura et al., 2010), the calculated transition pressures and temperatures for Al5 (*i.e.*, 2700 ppm wt. H_2O) match those expected for seismic scatterers detected at 720 or 860 km depth, for instance, underneath the Fiji-Tonga and South American subduction zones. The shallower occurrence of seismic scatterers in deep subduction settings seems, therefore, compatible with the presence of reservoirs of hydrous basaltic crust being recycled into the deep lower mantle.

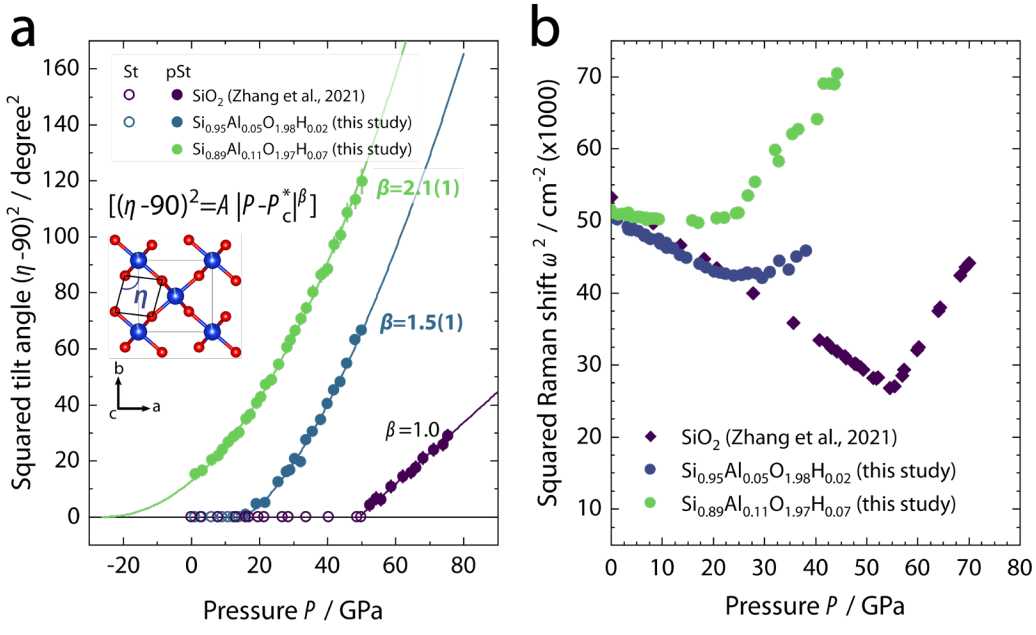

Figure 3 a) *Pressure evolution of the squared octahedral tilt angle [(η – 90)²] in SiO_2 and H,Al-bearing stishovite (St) and post-stishovite (pSt), and power law fits to the experimental data. The exponent β is reported next to each curve. In the inset, crystal structure of post-stishovite highlighting the tilting of the octahedra.* ***b)*** *Pressure dependence of the squared Raman mode in SiO_2 and H,Al-bearing stishovite.*

COMPRESSIBILITY OF DENSE HYDROUS SILICATE AL-PHASE D

Out of the hydrous phases that have been proposed to carry water in the mantle transition zone and topmost lower mantle, the Al-rich end member of DHMS phase D, nominally $Al_2SiO_6H_2$, was found to be the most resilient to the high temperatures of the ambient mantle, possibly due to its strong H-bonds (Pamato et al., 2015). The effect of Al substitution on the elastic properties of phase D samples remains, however, controversial.

Here, the first experimental constraints on the crystal structure and compressibility of a synthetic $Al_{1.53(2)}Fe^{3+}_{0.22(1)}Si_{0.86(1)}O_6H_{3.33(9)}$ Al-phase D sample are presented. Single-crystal X-ray diffraction measurements in the DAC were conducted at the ECB P02.2 (Petra-III, Hamburg, Germany) over two runs between room pressure and 52 GPa. A fit of the experimental data up to 38 GPa yielded a K_0 value that falls toward the higher range of previously proposed parameters for Mg-phase D. No evidence for elastic stiffening due to the symmetrization of H-bonds was found in this pressure interval, suggesting that the strength of H-bonds and their symmetrization do not affect the compressibility of Al-phase D.

Above 38 GPa, a change in the compression behavior was observed because of a high-to-low spin crossover of octahedrally coordinated Fe^{3+}, as reported by previous studies (*e.g.*, Wu et al. 2016). Despite the limited number of data points at these pressures, a recently proposed formalism was adopted, which makes use of crystal field parameters and their volume-dependency to calculate the energy associated with the high-spin and low-spin electronic states, from which the electronic energy and its derivatives can be calculated (Buchen, 2021). An inversion of all data from room pressure to 52 GPa shows excellent agreement with the experimental data points and suggests that the spin crossover region extends between approximately 35 and 65 GPa (Fig. 4), in good agreement with some previous studies.

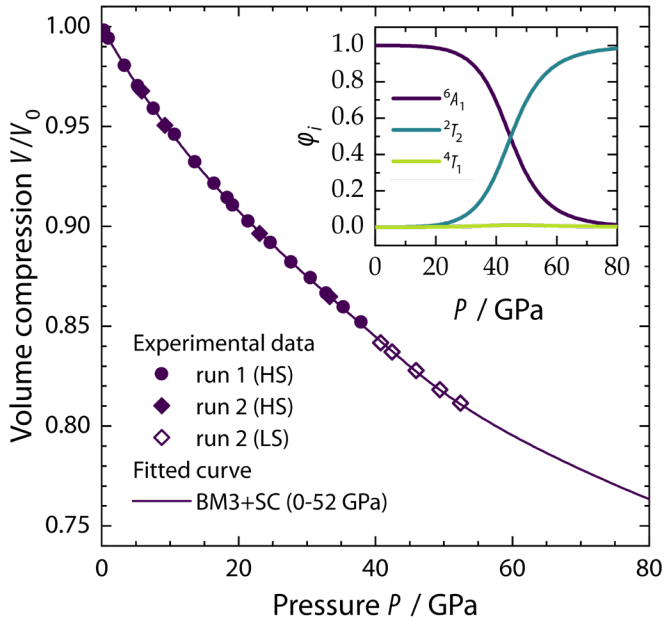

Figure 4 *Volume compression data of Fe-bearing Al-phase D and fitted spin-crossover (SC) 3rd-order Birch-Murnaghan (BM3) equation of state across the Fe^{3+} high-spin (HS) to low-spin (LS) crossover region. In the inset, the fraction (φ) of electrons in the HS ($^6A_1$) and LS ($^2T_2$, $^4T_1$) states is modelled as a function of pressure using the same BM3+SC fit parameters used to model the equation of state.*

Despite phase D solid solution displaying a wide range of K_0 and K'_0 values at room pressure, such a variability vanishes almost completely at ~20 GPa, where phase D is expected to be stable, due to the anti-correlation of the proposed K_0 and K'_0. Therefore, at the mantle transition zone and topmost lower mantle pressures, the bulk modulus of phase D solid solution is expected to be weakly affected by crystal chemical substitutions.

REFERENCES

Brodholt, J.P. (2000) - Pressure-induced changes in the compression mechanism of aluminous perovskite in the Earth's mantle. Nature, 407, 620–622.

Buchen, J. (2021) - Seismic Wave Velocities in Earth's Mantle from Mineral Elasticity. In: "Mantle Convection and Surface Expressions", H. Marquardt, M. Ballmer, S. Cottaar, J. Konter, eds. American Geophysical Union, 51-95.

Dziewonski, A.M. & Anderson, D.L. (1981) - Preliminary reference Earth model. Phys. Earth Planet. In., 25, 297–356.

Frost, D.J. (2006) - The Stability of Hydrous Mantle Phases. Rev. Mineral. Geochem., 62, 243–271.

Huang, R., Boffa Ballaran, T., McCammon, C.A., Miyajima, N., Dolejš, D., Frost, D.J. (2021) - The composition and redox state of bridgmanite in the lower mantle as a function of oxygen fugacity. Geochim. Cosmochim. Ac., 303, 110–136.

Ishii, T., Criniti, G., Ohtani, E., Purevjav, N., Fei, H., Katsura, T., Mao, H.K. (2022) - Superhydrous aluminous silica phases as major water hosts in high-temperature lower mantle. P. Natl. Acad. Sci. USA, 119, 1–6.

Kaneshima, S. (2019) - Seismic scatterers in the lower mantle near subduction zones. Geophys. J. Int., 218, 1873–1891.

Kurnosov, A., Marquardt, H., Frost, D.J., Boffa Ballaran, T., Ziberna, L. (2017) - Evidence for a Fe3+-rich pyrolitic lower mantle from (Al,Fe)-bearing bridgmanite elasticity data. Nature, 543, 543–546.

Murakami, M., Ohishi, Y., Hirao, N., Hirose, K. (2012) - A perovskitic lower mantle inferred from high-pressure, high-temperature sound velocity data. Nature, 485, 90–94.

Nakajima, Y., Frost, D.J., Rubie, D.C. (2012) - Ferrous iron partitioning between magnesium silicate perovskite and ferropericlase and the composition of perovskite in the Earth's lower mantle. J. Geophys. Res.-Solid, 117.

Navrotsky, A., Schoenitz, M., Kojitani, H., Xu, H., Zhang, J., Weidner, D.J., Jeanloz, R. (2003) - Aluminum in magnesium silicate perovskite: Formation, structure, and energetics of magnesium-rich defect solid solutions. J. Geophys. Res.-Solid, 108.

Nomura, R., Hirose, K., Sata, N., Ohishi, Y., Suetsugu, D., Bina, C., Inoue, T., Wiens, D., Jellinek, M. (2010) - Precise determination of post-stishovite phase transition boundary and implications for seismic heterogeneities in the mid-lower mantle. Phys. Earth Planet. In., 183, 104–109.

Pamato, M.G., Myhill, R., Boffa Ballaran, T., Frost, D.J., Heidelbach, F., Miyajima, N. (2015) - Lower-mantle water reservoir implied by the extreme stability of a hydrous aluminosilicate. Nat. Geosci., 8, 75–79.

Stixrude, L. & Lithgow-Bertelloni, C. (2005) - Thermodynamics of mantle minerals - I. Physical properties. Geophys. J. Int., 162, 610–632.

Wu, X., Wu, Y., Lin, J.-F., Liu, J., Mao, Z., Guo, X., Takashi, Y., McCammon, C., Prakapenka, V.B., Xiao, Y. (2016) - Two-stage spin transition of iron in FeAl-bearing phase D at lower mantle. J. Geophys. Res.-Solid, 121, 6411–6420.

Zhang, Y., Fu, S., Wang, B., Lin, J.F. (2021) - Elasticity of a Pseudoproper Ferroelastic Transition from Stishovite to Post-Stishovite at High Pressure. Phys. Rev. Lett., 126, 25701.

Zhang, Y., Chariton, S., He, J., Fu, S., Xu, F., Prakapenka, V.B., Lin, J.F. (2023) - Atomistic insight into the ferroelastic post-stishovite transition by high-pressure single-crystal X-ray diffraction. Am. Mineral., 108, 110–119.